ISSN 1560-8034, 1605-6582 (On-line), SPQEO, 2020. V. 23, N 1. P. 60-65.

Hetero- and low-dimensional structures

Some features of Mn^{2+} EPR spectra in cubic nano-ZnS

I.P. Vorona[1], S.S. Ishchenko[1], S.M. Okulov[1], V.V. Nosenko[1,2*]

[1]V. Lashkaryov Institute of Semiconductor Physics, National Academy of Sciences of Ukraine, 45, prospect Nauky, 03680 Kyiv, Ukraine
[2]National University of "Kyiv-Mohyla Academy", 2, Skovorody str., 04070 Kyiv, Ukraine
[*]E-mail: vvnosenko@ukr.net

Abstract. Four ZnS nanopowders containing an uncontrolled impurity of manganese were studied using EPR technique. The powders with the average sizes (6…8 nm) were synthesized by either joint or sequential decomposition of diethyldithiocarbamate complexes of zinc and europium in high-boiling solvents at various temperatures. All samples demonstrated the EPR signal that is not typical for ZnS powders with μm-sized particles. Computer simulation showed that EPR spectra of all the samples could be fitted by two components. The first component with $g = 2.0022 \pm 0.0002$, $A = (-63.5 \pm 0.5) \cdot 10^{-4}\,\mathrm{cm}^{-1}$, $b_4^0 \geq 3.5 \cdot 10^{-4}\,\mathrm{cm}^{-1}$ was assigned to Mn^{2+} ions in the cubic surrounding, Mn(C). The parameters of the second component were $g = 2.0022 \pm 0.0002$, $A = (-63.5 \pm 0.5) \cdot 10^{-4}\,\mathrm{cm}^{-1}$, $b_2^0 = (-36 \pm 1) \cdot 10^{-4}\,\mathrm{cm}^{-1}$; this component was attributed to Mn^{2+} ions associated with a planar lattice defect (stacking fault), Mn^{2+}(D). The ratio of centers amounts Mn^{2+}(C)/Mn^{2+}(D) for the samples studied was 2.1/1 (in the samples 1 and 4) and 1.7/1 (in the samples 2 and 3), respectively. EPR of Mn^{2+} ions was shown to be an effective method for detecting planar lattice defects in ZnS nanoparticles.

Keywords: ZnS, EPR, paramagnetic defect, manganese ions, lattice structure.

https://doi.org/10.15407/spqeo23.01.60
PACS 76.30.-v, 81.07.Wx, 61.46.-w

Manuscript received 20.01.20; revised version received 24.02.20; accepted for publication 18.03.20; published online 23.03.20.

1. Introduction

Materials containing zinc sulfide nanoparticles (NPs) have a great potential for wide range of technical applications. In particular, nano-ZnS is promising for applications in thermoluminescent dosimetry and solar batteries [1], in light sources [2]. Zinc sulphide NPs also attract attention of researchers due to size-dependent physical properties, *e.g.*, blue shift of the fundamental absorption edge [3, 4], variation of the temperature of phase transition from the cubic to hexagonal structure [5, 6], enhancement of photoluminescence intensity, and low-voltage cathodoluminescence [7, 8]. ZnS NPs activated by various impurities are of particular interest, since doping essentially changes the properties of NPs. To elucidate the origin of these changes, the detailed study of the impurity centers structure, including impurity-related local distortions of the crystal lattice, is of utmost importance.

Many works have been devoted to nano-ZnS containing Mn^{2+} ions (see, *e.g.*, [9–14]). All these papers reported the EPR spectra of substitutional Mn ions (Mn_{Zn}^{2+}) in cubic nanoparticles, which differ from the spectra observed in μm-sized cubic ZnS particles. The authors of the published works either did not pay attention to these discrepancies, or used exotic sets of spin Hamiltonian parameters including anisotropic g and A tensors, as well as zero crystal field terms corresponding to axial or even rhombic local distortions. In [11], being based on an accurate lineshape analysis of the multifrequency EPR spectra, the parameters of Mn_{Zn}^{2+} in nanoparticles were determined. The obtained center parameters were similar to those observed earlier in the mixed polytype ZnS crystals containing both cubic and hexagonal phases [15, 16]. Based on the above findings, the authors interpreted the EPR signal as that of the substitutional Mn^{2+} associated with a planar packing defect.

Later, this model was corroborated by direct observation of staking faults by high-resolution TEM [12]. The authors of [11, 12] suggested a hypothesis that formation of the above centers is caused by penetration of manganese ions into nanoparticles along planar lattice defect and the preferential localization of the Mn^{2+} impurity at Zn^{2+} cation sites next to a stacking defect. At the same time, in [13] two types of paramagnetic centers were detected in nano-ZnS: the above complex defects and substitutional Mn^{2+} ions in undistorted cubic surroundings. In this paper, we study EPR spectra of manganese-containing nano-ZnS of different sizes, synthesized using different technological routes, and analyze the structure of Mn^{2+}-related centers in detail.

2. Materials and methods

The characteristics of the samples studied are listed in Table. The first column of the table shows the synthesis temperature of the samples. The second and third columns list the sizes of NPs, which were determined using transmission electron microscopy (TEM) and X-ray diffraction (XRD) methods. The samples 1 and 2 were synthesized by joint decomposition of diethyldithiocarbamate complexes of zinc and europium in high-boiling solvents; the processes differed only by the synthesis temperature. In both processes, europium was used as an activating impurity. The sample 3 was obtained using sequential decomposition of the above complexes. The sample 4 was synthesized similarly to the sample 3, but afterwards a shell of zinc sulfide was formed around NPs by further decomposition of the corresponding complexes. For the detailed description of the synthesis, see [17].

XRD studies were done using the powder diffractometer Thermo Techno ARL X'TRA in the Bregg geometry. Data were collected over the 2θ range 20…80°, with the steps 0.02°. The measurements were carried out at room temperature (wavelength $K_\alpha 1$ = 1.540562 Å, $K_\alpha 2$ = 1.544390 Å). For high-quality spectrum analysis, the Search Match software package was used. The particle sizes were determined using the Scherrer formula: $D_{hkl} = 0.9\lambda/\beta_{hkl}\cos\theta$, where λ is the radiation wavelength, β_{hkl} – full width of the reflection at half-maximum, θ denotes the angular position of the peak.

Photomicrographs were obtained using the Selmi PEM-125K transmission electron microscope under the accelerating voltage 100 kV. The average sizes of these nanoparticles were determined using the statistical analysis of sizes of more than 200 individual objects.

EPR spectra were recorded with a Varian E12 spectrometer at room temperature. To avoid distortion of EPR lines, the low microwave power (< 2 mW) and amplitude modulation 0.1 mT of magnetic field were used. EPR spectra were simulated using the POWDER program that is a part of the Visual-EPR software package [18], based on the algorithm described in [19]. The studied EPR spectra are caused by Mn^{2+} ions that are present in the NPs of ZnS as an uncontrolled impurity. EPR spectra of europium were not detected.

Table. Characteristics of the samples.

Sample	Synthesis temperature, °C	*d*, nm	
		TEM	XRD
1	300	7.0 ± 1.0	5.3 ± 1.0
2	240	6.0 ± 0.8	4.6 ± 1.0
3	240	6.2 ± 1.0	4.5 ± 1.0
4	240	7.7 ± 1.0	5.8 ± 1.0

3. Results and discussion

Usually, when manganese is incorporated into ZnS, it substitutes zinc and forms Mn^{2+} centers. To describe the EPR spectrum of this center, the spin-Hamiltonian (SH) containing electron and nuclear Zeeman terms, hyperfine term, and zero field splitting term (interaction of the electrons spin with crystal field) is generally used

$$H = g\beta\mathbf{BS} - g_N\beta_N\mathbf{BI} + A\mathbf{SI} + \sum_{n.m} f_n b_n^m O_n^m \ .$$

Here, we use the standard notations (*e.g.*, see [20, 21]). The values g, g_N, β, β_N, and A are assumed to be isotropic. The set of parameters b_n^m is defined by Mn^{2+} surrounding and depends on the type of ZnS lattice and its distortion. In macrocrystals of zinc sulfide, the Mn^{2+} center is studied well. Its EPR spectrum in the cubic crystal lattice is described by the following SH parameters: $g = 2.0022$, $A = -64.5\cdot10^{-4}\,\mathrm{cm}^{-1}$, $b_4^0 = 3.9\cdot10^{-4}\,\mathrm{cm}^{-1}$ [22]. In the hexagonal lattice the SH parameters are: $g = 2.0016$, $A = -65\cdot10^{-4}\,\mathrm{cm}^{-1}$, $b_2^0 = -105\cdot10^{-4}\,\mathrm{cm}^{-1}$, $3b_4^0 - 0.1b_4^3 = 7.6\cdot10^{-4}\,\mathrm{cm}^{-1}$ [23].

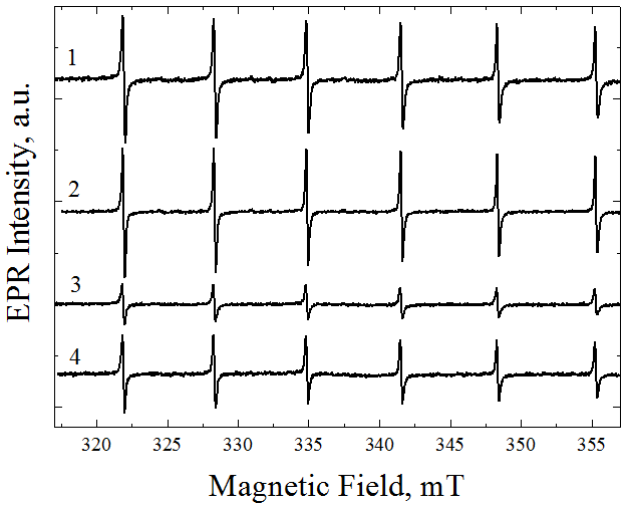

Fig. 1. EPR spectra of Mn^{2+} in nano-ZnS samples. The numbering of the spectra corresponds to that of the samples in the table.

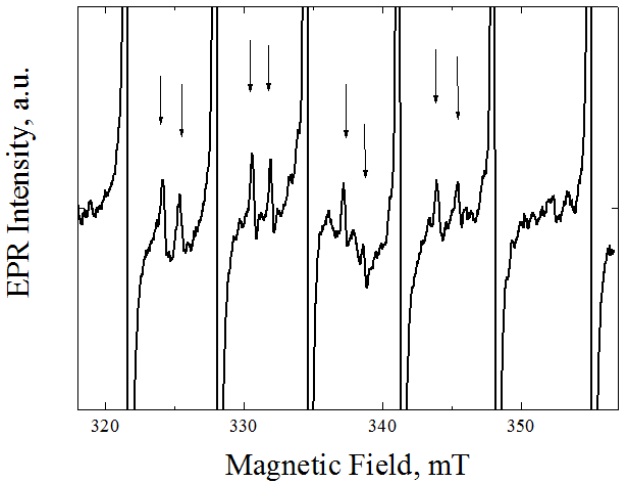

Fig. 2. EPR spectrum of the sample 2 at high amplification. The arrows indicate the lines of forbidden transitions.

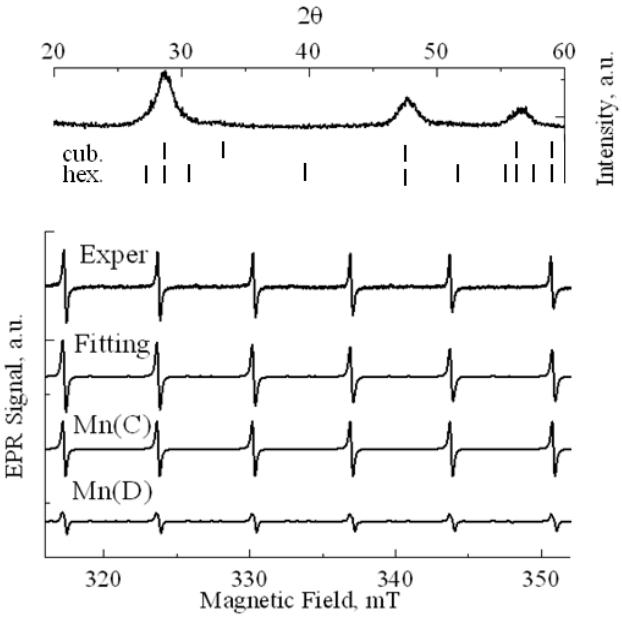

Fig. 3. Experimental and model EPR spectra of the sample 2. The fitting components, Mn^{2+}(C) and Mn^{2+}(D), are also shown. Upper part of Fig. 3 demonstrates the XRD spectrum for the sample 2. The positions of cubic and hexagonal zinc sulfide reflections are shown below.

The difficulties in studying the structure of nanomaterials by using the EPR method are related to the spatial averaging of the spectra originating from both allowed and forbidden transitions, as well as to possible local distortions of the crystal lattice. It should be noted that computer programs based on the second order perturbation theory do not give correct results when calculating EPR spectra of manganese in ZnS powders. To optimize the computer simulation of EPR spectra, it is important to understand the influence of certain parameters of the crystal field term on the resulting spectrum. In relation to Mn^{2+} in ZnS this problem has been studied in detail in [24]. It was found that, when b_4^0

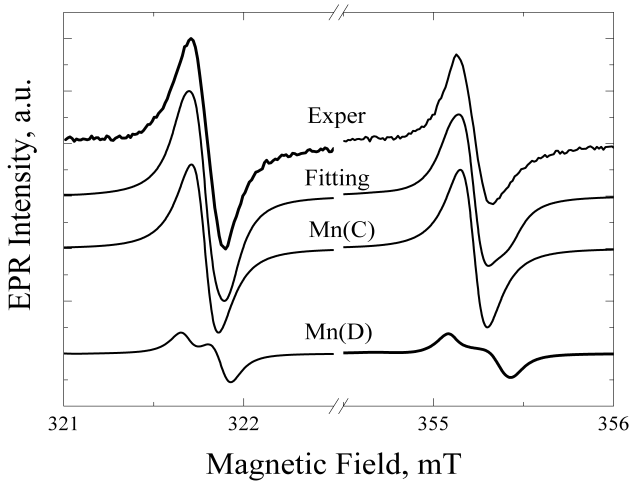

Fig. 4. Low-field and high-field lines of the experimental and model EPR spectra of the sample 2.

(cubic structure) prevails among the crystal field parameters, the sextet of equal intensity lines related to electronic transitions $\pm 1/2 \leftrightarrow \pm 1/2$ dominates in the spectrum. Forbidden transitions, as a rule, are not observed due to small value of b_4^0 parameter.

In the case when b_2^0 parameter dominates (which is characteristic of the hexagonal lattice), the spectrum is determined by the same sextet, but the amplitude of these sextet lines decreases with increasing the magnetic field induction. In addition, each of these lines splits and forms a doublet (or becomes broadened with a distorted lineshape); the splitting increases with increasing the magnetic field. Forbidden transitions are also observed.

The shape of EPR spectrum in hexagonal lattice strongly depends on the local crystal field parameter b_2^0 [24]. Thus, to determine SH parameters of the centers in mixed cubic-hexagonal powders based on the computer simulations of experimental data, the positions of the allowed and forbidden transitions as well as the line-shapes of the resonance lines must be taken into account.

Fig. 1 shows the EPR spectra of four samples listed in Table. The samples have the same mass, so the differences in the EPR intensities of corresponding samples are, most likely, caused by different concentrations of substitutional manganese. Although, at first glance, the spectra are similar to the powder EPR spectra of Mn^{2+} in a cubic structure, the detailed analysis reveals the above-mentioned features related to hexagonal structure. Namely, in all spectra the intensities of lines in sextets decrease with increasing the magnetic field, while their width and distortion of lineshape increase. Thus, the observed spectrum cannot be the signal of only one type of centers; the observed behavior points to the contribution of Mn ions in different structural positions, namely, those where the crystal field has an axial component ($b_2^0 \neq 0$). At high amplification, the forbidden transitions can also be seen (look at Fig. 2). We have done computer simulations of all the above spectra; an example of modeling is shown in Fig. 3 for the sample 2.

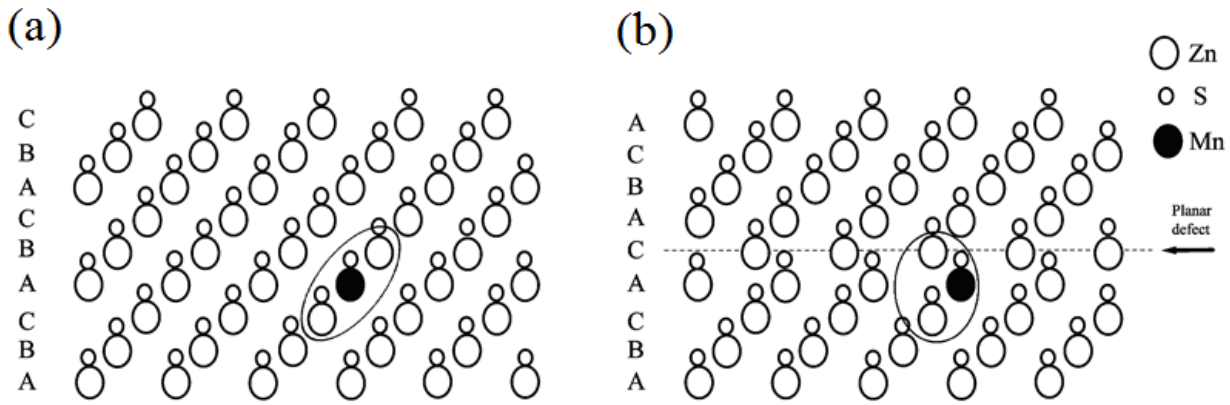

Fig. 5. Cubic structure of ZnS with the Mn^{2+} ions without a planar packing defect (a) and in the presence of this defect near Mn^{2+}(b). The nearest surrounding of Mn^{2+} is marked out with the oval.

Upper part of Fig. 3 demonstrates the XRD spectrum for the sample 2. The positions of cubic and hexagonal zinc sulfide reflections are shown by dashes. The reflections in the XRD spectrum are significantly broader as compared with those obtained for the powders that contain large particles. Despite the broadening, the XRD pattern can be ascribed to the cubic zinc sulfide. The XRD patterns of the samples 1, 3, 4 were similar to the XRD pattern of the sample 2 and did not demonstrate any significant differences. SH parameters were determined as based on the detailed fitting of lineshape (see Fig. 4). As a result, it was shown that each spectrum in Fig. 1 can be fitted by two components. The first component can be described by the parameters $g = 2.0022 \pm 0.0002$, $A = (-63.5 \pm 0.5) \cdot 10^{-4}\,\mathrm{cm}^{-1}$, $b_4^0 \geq 3.5 \cdot 10^{-4}\,\mathrm{cm}^{-1}$ and is attributed to substitutional Mn^{2+} ions located in the cubic environment – Mn^{2+} (C). The second component of EPR spectra has $g = 2.0022 \pm 0.0002$, $A = (-63.5 \pm 0.5) \cdot 10^{-4}\,\mathrm{cm}^{-1}$, $b_2^0 = (-36 \pm 1) \cdot 10^{-4}\,\mathrm{cm}^{-1}$. According to (Nistor *et al*. [12]), the latter component corresponds to the substitutional Mn^{2+} associated with the planar lattice defect – Mn^{2+}(D).

The ratio of amounts of these centers Mn^{2+}(C)/Mn^{2+}(D) in the studied samples was equal to 2.1/1 (samples 1 and 4) and 1.7/1 (samples 2 and 3). Fig. 5 shows the cubic structure of ZnS with the centers Mn^{2+}(C) (Fig. 5a) and Mn^{2+}(D) (Fig. 5b). As can be seen from Fig. 5b, when Mn^{2+} ion is situated nearby the planar lattice defect, an axial component appears in the crystal field of the ion's nearest surrounding. Therefore, for the modeling of Mn^{2+}(D) spectra the b_2^0 parameter and the appearance of the forbidden transitions must be taken into account. Note that the nearest surrounding of Mn^{2+}(D) coincides with the nearest surrounding of Mn^{2+} in the hexagonal structure of ZnS. The difference in the b_2^0 values for these cases is apparently caused by the substantial contribution to the crystal field of more distant coordination spheres that are not identical in distorted cubic and hexagonal lattices.

Previously in [11, 12], Mn^{2+}(D) centers were predominantly registered in Mn-doped nano-ZnS. Therefore, it was concluded that the planar lattice defects affected the manganese diffusion into NPs and caused the preferential localization of Mn^{2+} ions near these defects. In the studied nano-ZnS samples, both Mn^{2+}(D) and Mn^{2+}(C) centers were detected. Apparently, observation of Mn can be explained by the presence of an uncontrolled manganese impurity in the precursors and consequent incorporation of Mn into NPs during the growth process. As a result, manganese appears to be homogeneously distributed within NPs. In this case, the preferential formation of Mn^{2+}(D) centers should not be observed. It follows from the foregoing that the ratio Mn^{2+}(C)/Mn^{2+}(D) depends both on the number of planar lattice defects and on the way how manganese is incorporated into NPs. Different values of Mn^{2+}(C)/Mn^{2+}(D) for the samples studied are most likely related to different numbers of the planar defects.

The Mn^{2+} center, which is characteristic for the hexagonal structure, was not observed.

4. Conclusions

Four ZnS nanopowders containing an uncontrolled impurity of manganese have been studied. All the studied samples exhibited two EPR signals associated with Mn^{2+} ions. The first signal is described by the following parameters $g = 2.0022 \pm 0.0002$, $A = (-63.5 \pm 0.5) \cdot 10^{-4}\,\mathrm{cm}^{-1}$, $b_4^0 \geq 3.5 \cdot 10^{-4}\,\mathrm{cm}^{-1}$ and belongs to the manganese ions in the cubic ZnS, the Mn^{2+}(C) center. The second signal is characterized by $g = 2.0022 \pm 0.0002$, $A = (-63.5 \pm 0.5) \cdot 10^{-4}\,\mathrm{cm}^{-1}$, $b_2^0 = (-36 \pm 1) \cdot 10^{-4}\,\mathrm{cm}^{-1}$. The second signal is caused by Mn^{2+} ions associated with planar lattice packing defects, the Mn^{2+}(D) center. The ratio Mn^{2+}(C)/Mn^{2+}(D) for the studied samples was 2.1/1 (samples 1, 4), 1.7/1 (samples 2, 3), which, apparently, is due to the different numbers of planar defects in them.

The analysis of our experimental results and available literature data show that no EPR signal related to the substitutional Mn^{2+} ion in hexagonal crystal structure is observed in ZnS NPs. This finding apparently demonstrates that all ZnS NPs have a cubic crystal structure, regardless of production technology. Besides, the analysis has shown that all Mn^{2+} EPR spectra in nano-ZnS demonstrate the features inherent to Mn^{2+}(D) centers. Furthermore, these features were found in the EPR spectra of nano-ZnSe [25] and nano-CdS [26]. It indicates that the planar lattice defect is a common defect for nano-ZnS and occurs in other nanomaterials based on II-VI semiconductor crystals. This observation can be explained by formation of a stable (energy favorable) complex defect that includes substitutional Mn^{2+} ion and the stacking fault. This observation of Mn^{2+} EPR spectra allows researchers to control the presence of these complex defects (and, hence, the stacking fault) in NPs. This assumption is strongly supported by the observation of the stacking fault in undoped (Mn-free) nano-crystalline ZnS using high resolution TEM [27].

It is worth to note that there is a possibility that the stacking faults in nano-ZnS can associate with other (not manganese) impurities. These complex centers can significantly affect the optical, electrical and magnetic properties of the nanoscale material and, therefore, require further investigations.

Acknowledgements

This work is partially supported by Volkswagen Foundation and National Academy of Science of Ukraine (Project No. 26/18-H).

Reference

1. Bruchez M. Jr., Moronne M., Gin P., Weiss S., Alivisatos A.P. Semiconductor nanocrystals as fluorescent biological labels. *Science*. 1998. **281**. P. 2013–2016. https://doi.org/10.1126/science.281.5385.2013.
2. Luong B.T., Hyeong E., Yoon S., Choi J., Kim N. Facile synthesis of UV-white light emission ZnSe/ZnS:Mn core/(doped) shell nanocrystals in aqueous phase. *RSC Adv*. 2013. **3**. P. 23395–2340. https://doi.org/10.1039/C3RA44154G.
3. Bera D., Qian L., Tseng T.K., Holloway P.H. Quantum dots and their multimodal applications: A review. *Materials*. 2010. **3**. P. 2260–2345. https://doi.org/10.3390/ma3042260.
4. Vatankhah C., Ebadi A. Quantum size effects on effective mass and band gap of semiconductor quantum dots research. *J. Rec. Sci*. 2013. **2**. P. 21–24.
5. Qadri S.B., Skelton E.F., Hsu D., Dinsmore A.D., Yang J., Gray H.F., Ratna B.R. Size-induced transition-temperature reduction in nanoparticles of ZnS. *Phys. Rev. B*. 1999. **60**. P. 9191. https://doi.org/10.1103/PhysRevB.60.9191.
6. Dinsmore A.D., Hsu D.S., Qadri S.B., Cross J.O., Kennedy T.A., Gray H.F., Ratna B.R. Structure and luminescence of annealed nanoparticles of ZnS:Mn. *J. Appl. Phys*. 2000. **88**. P. 4985–4993. https://doi.org/10.1063/1.1314326.
7. Bhargava R.N., Gallagher D., Hong X., Nurmikko A. Optical properties of manganese-doped nanocrystals of ZnS. *Phys. Rev. Lett.* 1994. **72**. P. 416–419. https://doi.org/10.1103/PhysRevLett.72.416.
8. Dinsmore A.D., Hsu D.S., Gray H.F., Qadri S.B., Tian Y., Ratna B.R. Mn-doped ZnS nanoparticles as efficient low-voltage cathodoluminescent phosphors. *Appl. Phys. Lett.* 1999. **75**. P. 802. https://doi.org/10.1063/1.124518.
9. Gonzalez Beermann P.A., McGarvey B.R., Muralidharan S., Sung R.C.W. EPR spectra of Mn^{2+}-doped ZnS quantum dots. *Chem. Mater.* 2004. **16**. P. 915–918. https://doi.org/10.1021/cm030435w.
10. Kripal R., Gupta A.K. EPR and optical studies of ZnS: Mn nanoparticles. *Chalcogenide Lett*. 2010. **7**. P. 203–209.
11. Nistor S.V., Stefan M., Nistor L.C., Ghica D., Mateescu C.D., Barascu J.N. Lattice defect assisted incorporation of Mn^{2+} ions in cubic II-VI semiconductor quantum dots. *IOP Conf Series: Mater. Sci. Eng*. 2010. **15**. P. 012024. https://doi.org/10.1088/1757-899X/15/1/012024.
12. Nistor S.V., Stefan M., Ghica D., Nistor L.C. Nanosize induced effects in luminescent ZnS:Mn^{2+} quantum dots. *Rad. Meas*. 2013. **56**. P. 40–43. https://doi.org/10.1016/j.radmeas.2013.01.046.
13. Nosenko V., Vorona I., Grachev V. *et al*. The crystal structure of micro- and nanopowders of ZnS studied by EPR of Mn^{2+} and XRD. *Nanoscale Res. Lett*. 2016. **11**. P. 517. https://doi.org/10.1186/s11671-016-1739-4.
14. Murugadoss G., Ramasamy V. Synthesis and optical characterization of single phased ZnS: Mn^{2+}/CdS core–shell nanoparticles. *Spectrochimica Acta*. Part A. 2012. **93**. P. 70–74. https://doi.org/10.1016/j.saa.2012.02.074.
15. Buch T., Clerjaud B., Lambert B. Electron-paramagnetic-resonance study of $3d^5$ ions in mixed-polytype zinc sulfide. *Phys. Rev. B*. 1973. **7**. P. 184–191. https://doi.org/10.1103/PhysRevB.7.184.
16. Lambert B., Buch T., Clerjaud B. Axial impurity sites in mixed polytype ZnS/Mn^{+2}. *Solid State Commun*. 1972. **10**. P. 25–27. https://doi.org/10.1016/0038-1098(72)90339-0.
17. Selishchev A.V., Pavlishchuk V.V. Luminescence and spectral characteristics of zinc sulfide nanoparticles doped with Eu. *Theor. Exp. Chem.* 2016. **51**. P. 366–374. https://doi.org/10.1007/s11237-016-9437-y.

18. Grachev V.G. 2013, www.visual-epr.com.
19. Grachev V.G., Semenov Yu.G. Methods of computer treatment of EPR and ENDOR spectra. *Radiospectroscopy*. Perm, 1983. P. 163–171.
20. Altshuler S.A., Kozyrev B.M. *Electron Paramagnetic Resonance of Compounds of the Elements of the Intermediate Groups*. Nauka, Moscow, 1972 (in Russian).
21. Rudowicz C., Misra S.K. Spin-Hamiltonian formalisms in electron magnetic resonance (EMR) and related spectroscopies. *Appl. Spectrosc. Rev*. 2001. **36**. P. 11–63. https://doi.org/10.1081/ASR-100103089.
22. Title R.S. Electron paramagnetic resonance detection of lattice distortion in Mn^{2+}-doped II-VI compounds. *Phys. Rev.* 1963. **131**. P. 2503–2504. https://doi.org/10.1103/PhysRev.131.2503.
23. Keller S.P., Gelles I.L., Smith W.V. Paramagnetic resonance absorption in Mn-activated hexagonal ZnS. *Phys. Rev*. 1958. **110**. P. 850–855. https://doi.org/10.1103/PhysRev.110.850.
24. Vorona I.P., Grachev V.G., Ishchenko S.S., Baran N.P., Bacherikov Yu.Yu., Zhuk A.G., Nosenko V.V. Crystal structure determination of low-dimensional ZnS powders using EPR of Mn^{2+} ions. *J. Appl. Spectrosc.* 2016. **83**. P. 51–55. https://doi.org/10.1007/s10812-016-0241-1.
25. Yang B. The photoluminescent and magnetic properties of Mn^{2+} ions at the interface of core/shell mn-doped nanocrystals. *Int. J. Nanoparticles. Nanotech*. 2017. **3**. P. 009. https://doi.org/10.35840/2631-5084/5509.
26. Jadhav P.A., Panmand R.P., Patil D.R., Fouad H., Gosavi S.W., Kale B.B. Triangular CdS nanostructure: effect of Mn doping on photoluminescence, electron spin resonance, and magneto-optical properties. *J. Nanopart. Res.* 2017. **19**. P. 218. https://doi.org/10.1007/s11051-017-3903-x.
27. Huang F., Banfield J.F. Size-dependent phase transformation kinetics in nanocrystalline ZnS. *J. Am. Chem. Soc*. 2005. **127**. P. 4523–4529. https://doi.org/10.1021/ja048121c.

Authors and CV

Igor P. Vorona, Leading researcher at the V. Lashkaryov Institute of Semiconductor Physics, NAS of Ukraine, Doctor of Sciences. The area of his scientific interests includes EPR, ODMR and ENDOR spectroscopy, defects in solids.

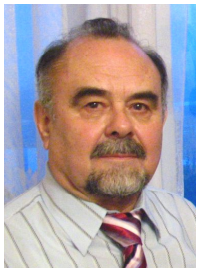

Stanislav S. Ishchenko, Consultant at the V. Lashkaryov Institute of Semiconductor Physics, NAS of Ukraine, Doctor of Sciences, Professor. The area of his scientific interests includes EPR and ENDOR spectroscopy, defects in solids.

Serhii M. Okulov, Senior Researcher at the V. Lashkaryov Institute of Semiconductor Physics, NAS of Ukraine. The area of his scientific interests includes EPR and ENDOR spectroscopy, defects in solids.

Valentyna V. Nosenko, Scientific Researcher at the V. Lashkaryov Institute of Semiconductor Physics, NAS of Ukraine. The area of her scientific interests includes EPR and ENDOR spectroscopy, defects in solids.